Polaron-Mediated Transport in $BiVO_4$ Photoanodes for Solar Water Oxidation

Hao Wu,[a,b] Lei Zhang,[c] Songying Qu,[a] Aijun Du,[c] Junwang Tang,[d] and Yun Hau Ng*[a]*

[a] Low Carbon and Climate Impact Research Centre, School of Energy and Environment, City University of Hong Kong, Kowloon, Hong Kong, People's Republic of China

[b] Present Address: Macao Institute of Materials Science and Engineering, Faculty of Innovation Engineering, Macau University of Science and Technology, Taipa, Macau, People's Republic of China

[c] School of Chemistry, Physics and Mechanical Engineering, Queensland University of Technology, Gardens Point Campus, Brisbane, QLD 4001, Australia

[d] Department of Chemical Engineering, University College London, Torrington Place, London WC1E 7JE, UK

AUTHOR INFORMATION

Corresponding Author

* Hao Wu - wuhao@must.edu.mo

* Yun Hau Ng - yunhau.ng@cityu.edu.hk

ABSTRACT. Hydrogen dopants and oxygen vacancies (OVs) play crucial roles in $BiVO_4$ photoanodes. However, the decisive factor determining the charge transport of the hydrogenated $BiVO_4$, particularly with electron small polaron formation remains elusive. Here we show a decreased charge transport barrier upon mildly hydrogenating the nanoporous $BiVO_4$ photoanode, as evidenced by the thermally-activating photocurrent responses. Monochromatic light photoelectrochemical performance, temperature-dependent conductivity, proton nuclear magnetic resonance, and density functional theory calculation disclose that the external hydrogen atoms occupy the intrinsic OVs in the $BiVO_4$, reducing the hopping activation energy and facilitating electron small polarons transport. The resulting $BiVO_4$ photoanode with $NiFeO_x$ cocatalyst achieves an applied-bias photo-to-current efficiency of 1.91 % at 0.58 V vs. RHE with front-illumination. This study extends the common understanding of the beneficial role in conventional donor density/surface chemisorption mediations of hydrogen doping to now include small polaron hopping.

TOC GRAPHICS

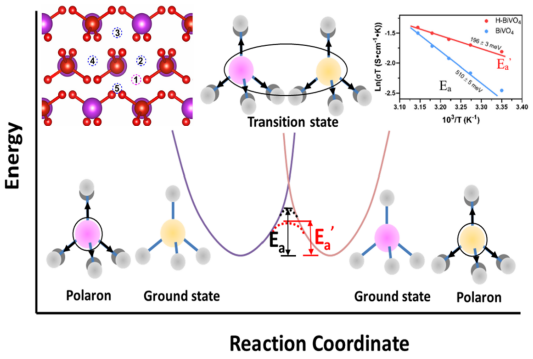

Bismuth vanadate ($BiVO_4$) is a potential photoactive semiconductor for photoelectrochemical (PEC) water splitting.[1–3] Its favorable band energy levels, visible light absorption, and low cost are attractive to practical applications.[4–6] Monoclinic $BiVO_4$ photoanode with a nanoporous structure developed by Kim et al. exhibited an excellent performance among the reported counterparts.[7,8] The hole charge transport inside the nanoporous $BiVO_4$ is no longer a limiting factor to the performance as its feature dimension is shorter than its hole charge diffusion length (~100 nm).[9] However, the ultimate performance of the $BiVO_4$ photoanode is still substantially hindered by its unsatisfactory charge transport, particularly by the low electron charge mobility originating from electron small polaron formations and a high density of intrinsic trapping states.[10] The electron small polaron is introduced by the surrounding lattice distortion confined to a region of the order of a unit cell, which hops from one site to the next with the help of lattice phonons, generally resulting in modest electron mobility (0.044 $cm^2\ V^{-1}\ S^{-1}$).[11]

Previous studies commonly performed the PEC tests of the $BiVO_4$ photoanodes under illumination with incident light directing to the FTO side (back-illumination) as the higher photocurrent density is observed compared with that of illuminated on the $BiVO_4$ side (front-illumination).[12] Recent studies disclosed that the lower front-illumination photocurrent density of $BiVO_4$ photoanodes is mainly caused by trap-limited electron transport (Figure 1a),[13] either due to electron-defect (trapping states) coupling or to electron-lattice (small polarons) coupling.[14] Therefore, front-illuminated $BiVO_4$ photoanodes with promising efficiencies are rarely reported, particularly on the optically thick $BiVO_4$ with nanoporous structure.[15–17]

Heteroatom doping and post-synthetic treatment have been demonstrated as two effective methods to tune the PEC performance of $BiVO_4$ photoanodes.[18–21] Inspired by the pioneering work of the hydrogenated TiO_2 reported by Chen et al.,[22] an analogous approach has been pursued for

$BiVO_4$ photoanodes.[23,24] The improved PEC activity was initially supposed to arise from the simultaneous formation of oxygen vacancies (OVs) acting as shallow trapping states donating electrons, thus increasing the conductivity.[25,26] However, Copper et al. revealed that the formed OVs via hydrogen doping likely act as deep trapping states with ~1.4 eV above the valence band of $BiVO_4$, severing the nonradiative charge recombination.[27] Yang et al. unraveled that the positively charged OVs could coulombically drag the electron small polaron hopping and lead to bound polarons, further decreasing the electron mobility of $BiVO_4$.[12] We argue that the constructive roles of OVs in PEC activity are subject to the condition that the OV density shall fall within the proper range. On the other hand, proton nuclear magnetic resonance (^{1}H NMR) studies disclosed that hydrogen doping generated substitutional hydrogen atoms at OVs and interstitial hydrogen in the $BiVO_4$, which act as shallow donors determining the n-type conductivity.[27,28] Although literature reported the crucial roles of hydrogen doping for $BiVO_4$ photoanodes, the conclusions of hydrogen dopants and OVs are still debatable and not fully understood at this stage. The decisive factor determining the charge transport of the hydrogenated $BiVO_4$, particularly with electron small polaron formation remains elusive.

This work develops an effective method to mildly hydrogenate $BiVO_4$ and revisits the polaron-mediated charge transport in low-temperature hydrogen-treated $BiVO_4$ photoanode. In addition to the improved charge transport and increased donor density generally documented in other literature, thermally-dependent photocurrent experiments suggest that the charge transport of the prepared $BiVO_4$ photoanode follows a hopping conduction mechanism, and the charge transport barrier is decreased upon hydrogen doping (Figure 1b). Monochromatic light PEC performance, temperature-dependent conductivity, ^{1}H NMR, and density functional theory (DFT) calculation further unravel that the electron small polaron hopping barrier near OVs of the $BiVO_4$ is decreased

by mild hydrogen doping, and the liberated polaron hopping is likely due to the filling of OVs with substitutional hydrogen dopants.

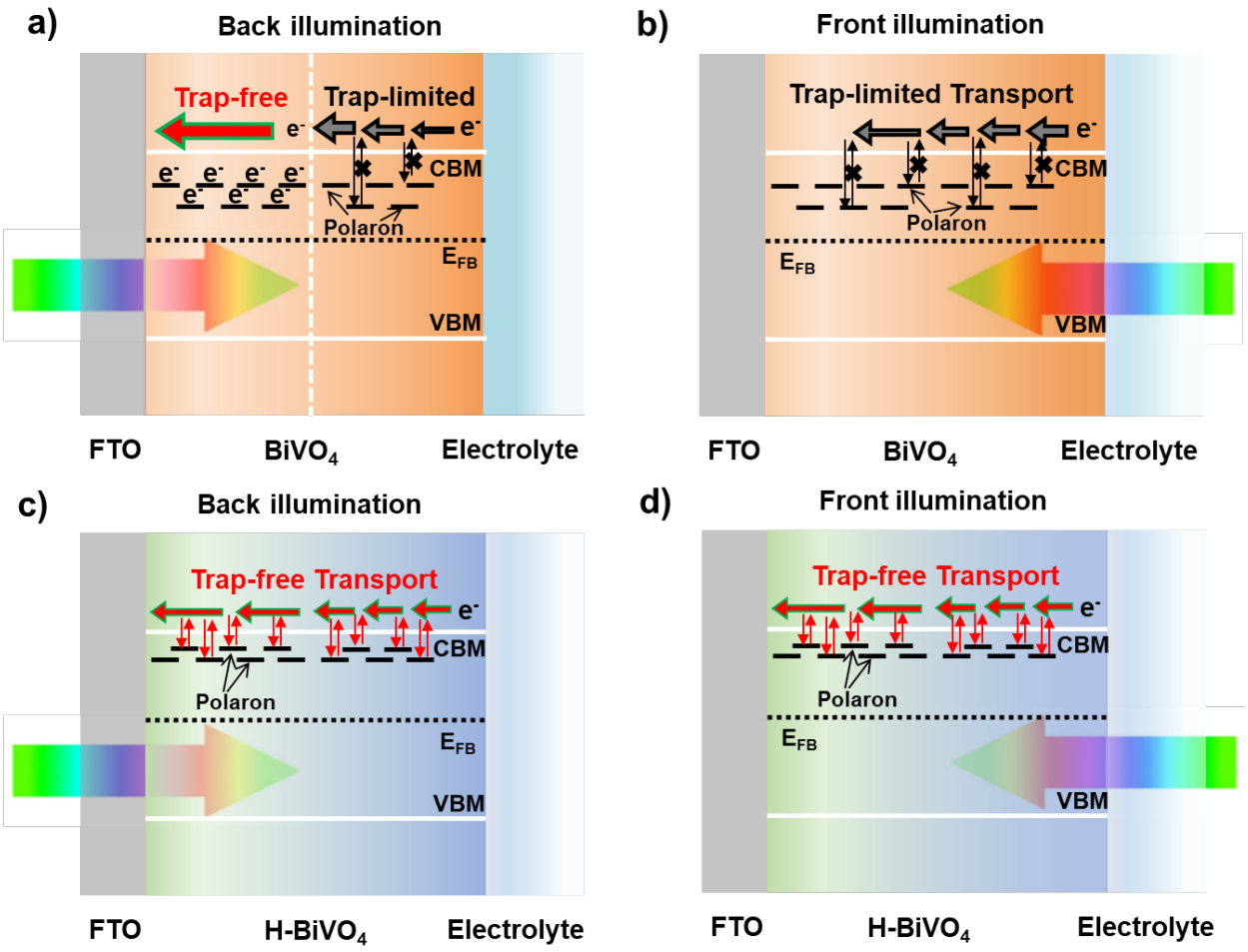

Figure 1. Schematic illustration of the electron transport processes in a) pristine $BiVO_4$ and b) hydrogenated $BiVO_4$ photoanode with the back and front illumination.

The nanoporous $BiVO_4$ thin films on the FTO substrate were synthesized using the method developed by Kim et al. (details in the Experimental Section).[7] The hydrogen doping on the $BiVO_4$ photoanodes was conducted in a sealed reactor with controlled pressure and temperature for 10 min. The treated samples are denoted as H-$BiVO_4$-(N_2 (bar): H_2 (bar), temperature). For example,

the $BiVO_4$ photoanode hydrogenated at 180 °C in the gas mixture of N_2 (2.0 bar) and H_2 (1.0 bar) is denoted as H-$BiVO_4$-(2.0:1.0, 180 °C). The morphology, electrochemically active surface area, crystalline phase, and light absorption properties of $BiVO_4$ were not affected by the mild hydrogen doping (Figure S1-S4, detailed descriptions in the Supporting Information). The effects of hydrogen doping on the chemical states and defects induction of the $BiVO_4$ were then characterized by X-ray photoelectron spectroscopy (XPS), electron paramagnetic resonance (EPR), and low-temperature photoluminescence (PL) experiments (Figure S5a-d, detailed descriptions in the Supporting Information). [29-31]

The PEC studies of the hydrogenated and pristine $BiVO_4$ photoanodes with front and back illumination were investigated in 1 M KBi solution (pH=9.5) under AM 1.5G light illuminance (100 mW cm^{-2}). The hydrogen partial pressure and the treatment temperature were optimized based on the front-illumination photocurrent densities (Figures S6a and b), and the pressure of N_2:H_2 (2.0:1.0) together with the temperature of 180 °C was chosen for further PEC water splitting studies. Moreover, the hydrogenated $BiVO_4$ photoanodes treated by the *Parr* reactor at different hydrogen partial pressures and treatment temperatures show a clear trend in photocurrent change, indicating better controllability in hydrogenation by the *Parr* reactor compared to the traditional annealing treatment.[27]

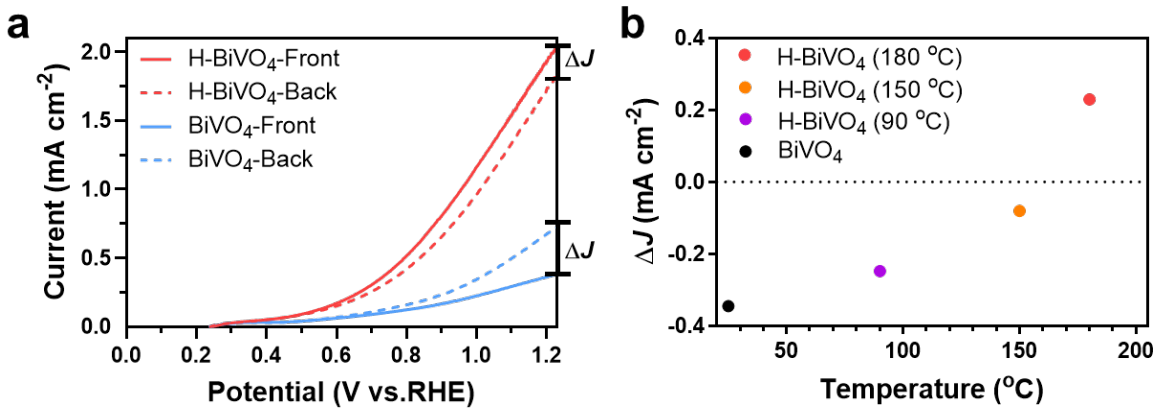

Figure 2. (a) Current density-voltage (*J-V*) curves of pristine $BiVO_4$ and H-$BiVO_4$-(2.0:1.0, 180 °C) photoanodes measured under AM 1.5G simulated light illumination in 1 M KBi solution. (b) The difference of current density (ΔJ) at 1.23 V vs. RHE between front and back illumination determined from the *J-V* curves against the hydrogen treatment temperature.

The H-$BiVO_4$-(2.0:1.0, 180 °C) photoanode shows an increase of front-illumination photocurrent density (J_{H2O}) of 2.05 ± 0.02 mA cm^{-2} at 1.23 V vs. RHE (Figure 2a), which is ~5.4 times of the pristine $BiVO_4$ (0.38 ± 0.03 mA cm^{-2}). For the pristine $BiVO_4$ photoanode, the photocurrent density with back-illumination (0.75± 0.02 mA cm^{-2}) was about twice that of front-illumination. The effective attenuation length of the incident light was determined to be 450 nm for monoclinic $BiVO_4$ according to Lambert-Beer's law.[13] The film thickness of 1 μm for the prepared $BiVO_4$ is therefore optically thick. The observed inferior front-illumination PEC performance of pristine $BiVO_4$ is consistent with the thickness-dependent photocurrent results in the literature.[13] Intriguingly, the H-$BiVO_4$-(2.0:1.0, 180 °C) photoanode exhibited a reverse trend with an even ~20% higher photocurrent density under the front-illumination than the back-illumination. Moreover, the narrowed gap in photocurrent densities for front- and back-illuminated $BiVO_4$ photoanode suggests that the charge transport has been greatly improved after the mild hydrogen treatment, which is also consistent with the literature.[31] To our knowledge, few reports could achieve the reverse trend by post-synthetic treatment in switching the originally inferior front-illumination system of optical thick $BiVO_4$ photoanode into a more superior system as compared with the back-illumination.[13] On the other hand, for the over-treated $BiVO_4$ photoanode (with the hydrogen treatment duration of 24 h), the photocurrent density is significantly decreased and even lower than that of the pristine $BiVO_4$ (Figure S6c). This deteriorated phenomenon is usually caused by the over-introduction of trapping defects by hydrogen impurities. The results

suggest that the effect of hydrogen doping on the charge transport of $BiVO_4$ is rather complex and the delicate control of hydrogen doping level is important.

To prove the effect of mild hydrogen doping on the difference of photocurrent density with front and back illumination (ΔJ), the results of the pristine $BiVO_4$ and hydrogenated $BiVO_4$ photoanodes treated at different temperatures (90 °C, 150 °C, and 180 °C) are shown in Figure 2b and Figure S7a-d. The ΔJ was initially negative (indicating photocurrent density of front-illumination being poorer than that of back-illumination), and the magnitude of the difference was sequentially reduced with raising the treatment temperature ($\leq$ 150 °C). The ΔJ turned positive at 0.21 mA cm^{-2} for the hydrogenated $BiVO_4$ photoanode treated at 180 °C. The lower front-illuminated performance of the optically thick $BiVO_4$ photoanode had been widely reported in the literature, which is likely due to the bounded electron transport.[27] From the front-side illumination, since the predominant charge carriers generation happens away from FTO substrate, the charge collection of photoinduced electrons is less efficient than that from the back-illumination caused by the trap-limited electron transport and the resulting short electron diffusion length (Figure 1a).[13] Given that only ~80% of light (350-600 nm) could pass through FTO (Figure S8), it is reasonable to expect a higher photocurrent density with front-illumination after suppressing the bounded electron transport in the optically thick $BiVO_4$ photoanodes. These results suggest that the mild hydrogen doping mediates the charge transport of $BiVO_4$ photoanodes, enabling a more efficient front-illuminated performance. The improvements in charge separation (η_{sep}), incident photon-to-current efficiency (IPCE), absorbed photo-to-current conversion efficiency (APCE), and surface charge injection efficiency (η_{inject}) for $BiVO_4$ photoanodes upon the mild hydrogen treatment were further conducted in 1 M KBi solution with a hole scavenger of SO_3^{2-} (Figure S9-S11, detailed descriptions in the Supporting Information).

Pioneering studies have suggested that the poor electron transport has limited the front-illumination performance of optically thick $BiVO_4$.[32] Experimental evidence from monochromatic light PEC studies supports the different electron transport efficiencies of the pristine and hydrogenated $BiVO_4$ photoanodes. Figure 3a shows the photocurrent of the hydrogenated $BiVO_4$ photoanode with a film thickness of >1 μm at 1.23 V vs. RHE under front monochromatic light illumination (440 nm and 490 nm) with different light intensities ranging from 0 to 1.2 mW. The photocurrent was linearly enhanced with an increase of light intensity.[33] As the optically thick $BiVO_4$ film can fully absorb the incident light, the concentrations of photogenerated electron-hole pairs are almost the same when the sample is excited with the same photon fluxes. In this situation, the effective attenuation length of the incident light at a wavelength of 440 nm is shorter than that of 490 nm. The region of photoinduced electron incident at 440 nm is further away from the $BiVO_4$/FTO interface compared with the 490 nm light under front-illumination. It means that the photoinduced electrons have to pass through a longer distance to reach the FTO substrate incident at 440 nm than 490 nm.[33,34] Even so, the photocurrent obtained by 440 nm excitation is even higher than that by 490 nm excitation for the hydrogenated BVO_4 photoanode. The higher photocurrent measured by the shorter-wavelength excitation from the front-side could be ascribed to the longer electron-diffusion length and higher electron-collection efficiency after hydrogen doping. On the other hand, the relationship is reversed, in which higher photocurrent is obtained by 490 nm excitation for the pristine $BiVO_4$ photoanode (Figure 3b), indicating its intrinsically poor electron transport. The same trend was also observed under different light-intensity excitations.

Furthermore, the photocurrents measured under the front and back monochromatic light illumination (440 nm) with different light intensities were also studied for the hydrogenated and pristine $BiVO_4$ photoanodes (Figures 3c and d). The hydrogenated $BiVO_4$ photoanode shows

higher photocurrents under front monochromatic light illumination than under back-illumination, and their photocurrent increases along with the light intensity (linear slopes). On the other hand, the pristine $BiVO_4$ photoanode shows a much inferior photocurrent with front-illumination than back-illumination under identical situations. The linear slope of the front-illuminated photocurrent is also much smaller than the back-illumination. These findings suggest that the electrons with high mobility produced by front-side light excitation on the hydrogenated $BiVO_4$ photoanode can be efficiently transported to the conductive substrate, resulting in a significant enhancement in photocurrent generation than the pristine $BiVO_4$ photoanode. The corresponding current-voltage curves are given in Figure S12a-c, indicating the same trend in wider anodic potentials.

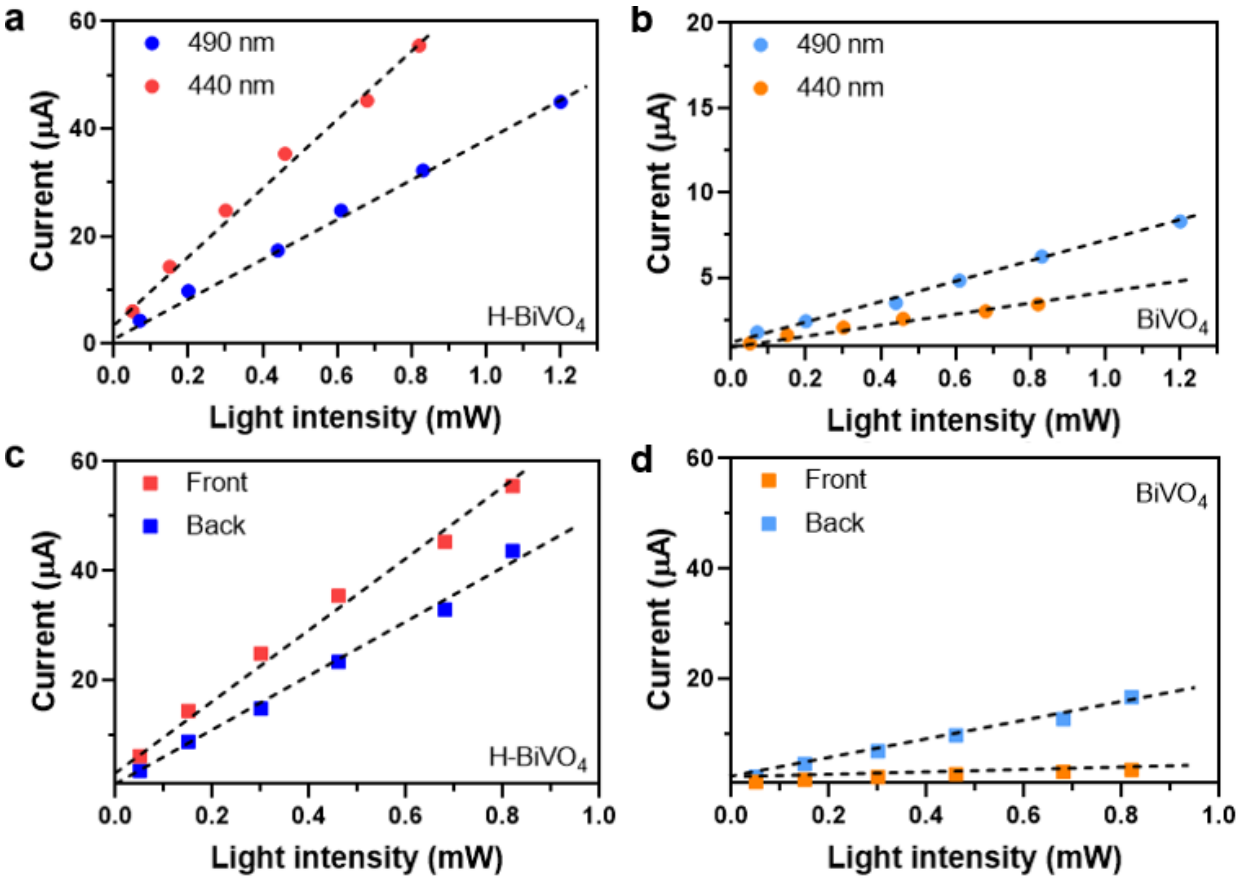

Figure 3. Photocurrent at 1.23 V vs. RHE of (a) H-$BiVO_4$-(2.0:1.0, 180 °C) photoanode and (b) pristine $BiVO_4$ photoanode under monochromatic light (440 nm and 490 nm) with different light intensities from the front-illumination. Photocurrent at 1.23 V vs. RHE of (c) H-$BiVO_4$-(2.0:1.0, 180 °C) photoanode and (d) pristine $BiVO_4$ photoanode under monochromatic light (440 nm) with different light intensities from front and back illumination.

The charge transit time, diffusion coefficient, and mobility of $BiVO_4$ photoanodes with front and back illumination are comparatively evaluated from the electrochemical impedance spectroscopy (EIS) results (Figures S13a and b, calculation details in the Supporting Information).[35,36] The calculated results show that the hydrogenated $BiVO_4$ photoanode with front-illumination has the shortest τ_d of 13.0 μs with the D_n of 7.67 x 10^{-6} cm^2 s^{-1} and μ_n of 2.99 x 10^{-4} cm^2 V^{-1} s^{-1}. For the H-$BiVO_4$-(2.0:1.0, 180 °C) photoanode with back-illumination, the τ_d, D_n, and μ_n are calculated to be 34.3 μs, 2.91 x 10^{-6} cm^2 s^{-1}, and 1.16 x 10^{-4} cm^2 V^{-1} s^{-1}, respectively. The results suggest that the hydrogenated $BiVO_4$ has better charge transport under front-illumination than back-illumination. On the other hand, this relationship is reversed for the pristine $BiVO_4$. The τ_d, D_n, and μ_n for the pristine $BiVO_4$ under back/front illuminations are determined to be ca. 109.0/163.0 μs, 0.92 x 10^{-6}/0.61 x 10^{-6} cm^2 s^{-1}, and 0.37 x 10^{-4}/0.23 x 10^{-4} cm^2 V^{-1} s^{-1}, respectively, indicating the intrinsically poor charge transport under front-illumination for the pristine $BiVO_4$ photoanode. The results suggest that the mild hydrogen doping by *parr* reactor improves the charge transport with increased charge mobility and relative charge diffusion length of $BiVO_4$ photoanode.[28]

We are now in a position to understand the underlying reasons for the improved charge transport, which reverses the originally inferior front-illumination system of optical thick $BiVO_4$ photoanode into a superior system than that with back-illumination. As shown in Figure 4a-c, both the H-

$BiVO_4$-(2.0:1.0, 180 °C) and pristine $BiVO_4$ photoanodes show that the photocurrent densities increase with temperature exponentially in an Arrhenius manner. The onset potential successively shifted to a positive direction with raising the temperature due to increased surface charge recombination as reported for Ti-doped Fe_2O_3 and Mo-doped $BiVO_4$.[14,33] In Figure 4c, the activation energy obtained from Arrhenius-type plots of ln$J$ vs. 1/T at 1.0 V vs. RHE for the H-$BiVO_4$-(2.0:1.0, 180 °C) photoanode (293 ± 3 meV) is smaller than that of the pristine $BiVO_4$ photoanode (532 ± 5 meV). In most photovoltaic and PEC cells, thermal energy usually lowers the photon-to-current conversion efficiency for band conductors with delocalized electron-hole pairs, causing a slightly decreased electron mobility with raising the temperature.[14,37] In contrast, the charge transport is expected to improve with temperature increase exponentially in an Arrhenius manner for transition metal oxides with localized charge carriers conducting through a hopping mechanism.[9] In these regards, the above results suggest that the charge carriers of the prepared $BiVO_4$ photoanodes with or without hydrogen doping follow a hopping conduction mechanism, and the activation barrier for photoinduced charge carriers hopping is decreased upon mild hydrogen doping.

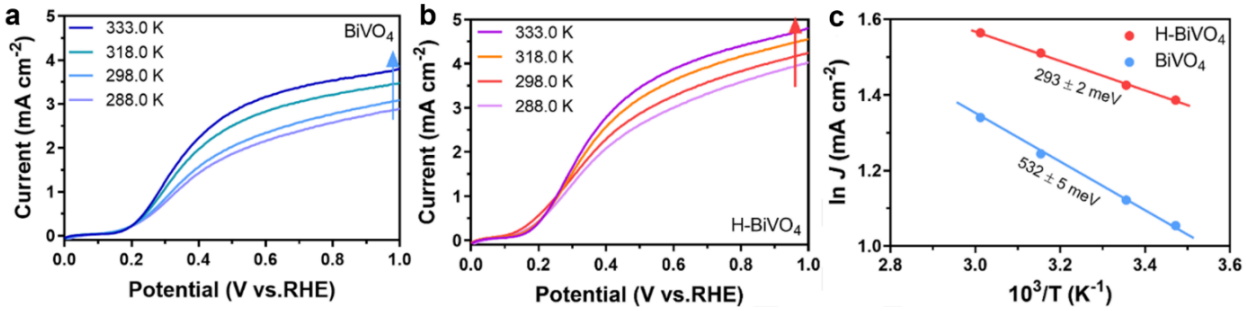

Figure 4. *J-V* curves of (a) pristine $BiVO_4$ and (b) H-$BiVO_4$-(2.0:1.0, 180 °C) photoanode measured in 1 M KBi solution with 0.5 M Na_2SO_3 at different temperatures. (c) Arrhenius

plots of ln*J* vs. 1/*T* at 1.0 V vs. RHE acquired for pristine $BiVO_4$ and H-$BiVO_4$-(2.0:1.0, 180 °C) photoanodes.

The electron transport in $BiVO_4$ is assumed to follow a small polaron hopping mechanism.[38,39] The electrons self-trapped in the surrounding lattice require thermal vibration to energize the trapped electrons to hop from one site to the next.[40,41] The energy required for this process is known as the hopping activation energy (E_a). The E_a gives rise to Arrhenius-type conductivity, which increases quasi-exponentially with temperature. The temperature-dependent conductivity measurement was performed to support the promoted polaron hopping with the decreased E_a upon mild hydrogen doping. We have fitted the ac conductivity ($\sigma'(\omega)$) spectra using Jonscher's power law by the equation $\sigma'(\omega) = \sigma_{d.c.} + A(T)\omega^n$, where the exponent, n, generally ranges between 0 and 1, and the $A(T)$ is the temperature-dependent frequency pre-exponential factor.[42–45] There is close agreement between the experimental and fitted data (Table S1 and S2) with the squared coefficient of linear correlation coefficient (R^2) close to 1.0, as also shown in the inset of Figure 5b for the H-$BiVO_4$-(2.0:1.0, 180 °C) photoanode at 318.0 K. The conductivities of the pristine and hydrogenated $BiVO_4$ photoanodes were increased with raising the temperature (Figure 5a and b). The *n* values ranged from 0.70 to 0.75, suggesting the small polaron transport behavior.[41] The *n* value should be equal to zero if the charge carriers are delocalized and free to drift through the bulk $BiVO_4$.

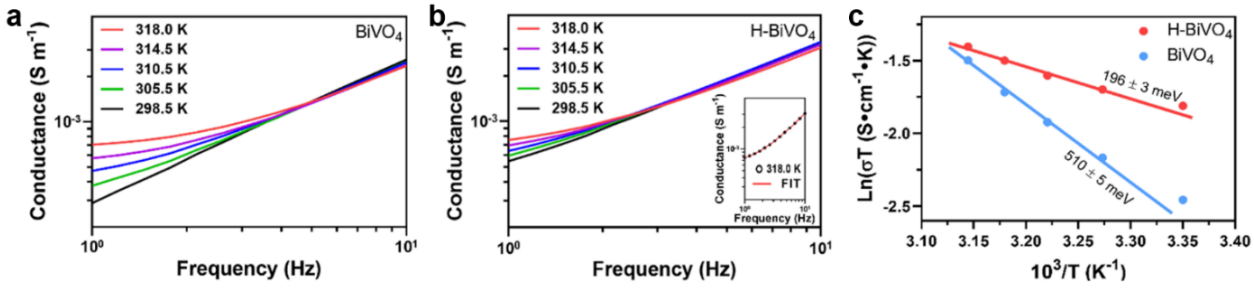

Figure 5. The real part of conductance plots as a function of frequency at different temperatures for (a) the pristine $BiVO_4$ and (b) the H-$BiVO_4$-(2.0:1.0, 180 °C) photoanodes. Inset: fitted ac conductivity plot at 318.0 K for the H-$BiVO_4$-(2.0:1.0, 180 °C) photoanode. (c) Conductivity fitting plots of the pristine $BiVO_4$ and H-$BiVO_4$-(2.0:1.0, 180 °C) photoanodes based on the small polaron transport model.

Moreover, the E_a of $BiVO_4$ photoanodes can be derived from the equation $\sigma(T) = AT^{-1}\exp(-E_a/k_BT)$, where $\sigma(T)$ is the conductance at a particular temperature (T) and A is a constant. As further determined from the $\ln[\sigma(T)\times T]$ - $1/T$ plots (Figure 5c), the E_a of $BiVO_4$ decreases from 510 ± 5 meV to 196 ± 3 meV after hydrogen doping. These values of E_a are comparable to other experimental and theoretical calculations of the small polaron hopping barrier of $BiVO_4$ photoanode in the literature.[41,46] The smaller E_a in the hydrogenated $BiVO_4$ means that electrons require less energy to hop from one $BiVO_4$ lattice site to the next, which arises from the changes in the coordination environment induced by the hydrogen dopant. We note that the activation energy of hole polaron hopping in $BiVO_4$ has been experimentally and theoretically proved to be much smaller than that of the electron small polaron hopping. It is about ~90 meV for hole polaron hopping. Our temperature-dependent conductivity measurements suggest that the hopping barrier of $BiVO_4$ photoanodes is much larger than 90 meV, which is closer to the electron small polaron hopping barrier (several hundreds of meV) as also shown in the literature.[40,41] Hence, such a high E_a of the pristine $BiVO_4$ is most likely caused by the electron small polaron hopping, which is the limiting factor in achieving the higher front-illumination performance of optically thick $BiVO_4$ photoanodes.

Table 1. Computationally calculated polaron hopping barriers (in eV) from defect site (D) to 1st nearest V atom site (N_{1st}) and from N_{1st} atom site to 2nd nearest V atom site (N_{2nd}).

		Path 1	Path 2	Path 3	Path 4	average
O_V	D-N_{1st}	0.413	0.660	0.473	0.656	**0.550**
	N_{1st}-N_{2nd}	0.539	0.483	0.484	0.364	**0.467**
O_V+H	D-N_{1st}	0.460	0.456	0.407	0.457	**0.445**
	N_{1st}-N_{2nd}	0.281	0.269	0.335	0.281	**0.292**

Computational studies uncover further investigations on the variation of polaron hopping behavior of $BiVO_4$ photoanodes with and without hydrogen dopants. Before the theoretical simulation of small polaron movement, the position of external hydrogen dopants in the $BiVO_4$ lattice was again testified by calculating the formation energies at different sites and ^1H NMR analysis (Figure S14a and b, detailed descriptions in the Supporting Information). Pioneering works by Rettie et al.[9] and Walsh et al.[47] disclosed that the electron small polarons are localized at V sites and could result in a partial occupation change from V^{5+} to V^{4+}, forming a stable electronic configuration in this transient chemical state. In this regard, the diagram in Figure S14c shows only V atoms for clarity, and one OV site was introduced near the V atom site. The polaron hopping paths from the V site with OV (defect site) to the 1st nearest V atom site (D → N_{1st}) and 1st nearest V atom site to the 2nd V atom site ($N_{1st} \rightarrow N_{2nd}$) are also illustrated in the diagram. The results show that the average hopping barrier from D → N_{1st} (550 meV) is larger than that from $N_{1st} \rightarrow N_{2nd}$ (467 meV) in the $BiVO_4$ lattice with an intrinsic OV (Table 1), which is consistent with previous reports suggesting that the positive charged OVs could coulombically bound small polarons.[41] On the other hand, when the OV site is occupied by an external hydrogen atom, the average small polaron hopping energy barriers are reduced. Notably, the average hopping barrier is decreased by 175 meV from $N_{1st} \rightarrow N_{2nd}$ upon the hydrogen substitution, which shows a 70 meV more decrease than D → N_{1st} pathways. It indicates that hydrogen dopant has a stronger

influence on the small polaron hopping at the site away from the defect site. Yang and coworkers have suggested that the charge transport barrier and the E_a in $BiVO_4$ are increased with the OV concentration, revealing that the OVs can act as trap centers and attract electron polarons to form more strongly bound polarons and result in lower mobility.[48] Therefore, the observed improved charge transport and PEC performance of hydrogenated $BiVO_4$ is likely owing to the hydrogen dopants occupying the intrinsic OVs with mediated small polaron hopping. The decreased small polaron hopping barrier could facilitate the charge transport with increased electron mobility (Figure S14d), suppressing the nonradiative recombination of photoinduced charge carriers along the pathway, thus improving the front-illumination performance of $BiVO_4$ photoanode.

Despite the improved charge transport, the J_{H2O} of the H-$BiVO_4$-(2.0:1.0, 180 °C) photoanode is still modest. $NiFeO_x$ was deposited on the photoanodes using a pulsed-photoelectrodeposition method (details in the Experimental Section). The $NiFeO_x$ cocatalyst improved the photocurrent density of H-$BiVO_4$-(2.0:1.0, 180 °C) photoanode to 4.68 mA cm^{-2} at 1.23 V vs. RHE with front-side illumination (Figure S15a), which is on par with the best performing $BiVO_4$ photoanodes (Table S3). Besides, the onset potential of $BiVO_4$ photoanode is negatively shifted by ~380 mV upon the deposition of $NiFeO_x$ due to the suppressed surface charge recombination.[19,49] The front illumination half-cell ABPE of the $NiFeO_x$/H-$BiVO_4$-(2.0:1.0, 180 °C) photoanode is determined to be 1.91% at 0.58 V vs. RHE (Figure S15b). The $NiFeO_x$/H-$BiVO_4$-(2.0:1.0, 180 °C) photoanode presented a vigorous water splitting process with Pt as the cathode in a gas-tight electrochemical cell (see Supplementary Video 1), at 0.58 V vs. RHE under AM 1.5G illuminance incident from the front-side. The amount of produced H_2 and O_2 gases was measured by gas chromatography and compared with calculated gas evolution from recorded photocurrent values shown in Figure S15c. The ratio of evolved H_2/O_2 was confirmed to be stoichiometric with a calculated Faraday

efficiency of 91% for O_2 evolution. Moreover, the $NiFeO_x$/H-$BiVO_4$-(2.0:1.0, 180 °C) photoanode showed a relatively stable photocurrent over 10 h operation (Figure S15d) and demonstrated the negligible change in physical properties after PEC reactions (Figure S16-17 and Table S4, detailed descriptions in the Supporting Information), indicating good durability of the system.

In summary, this work brought significant advancement to improve the front-illumination performance of optically thick $BiVO_4$ photoanodes and attempted to revisit the mediated charge transport dynamics of hydrogenated $BiVO_4$. We have reversed the originally inferior front-illumination system of an optically thick $BiVO_4$ photoanode into a more superior system than that under back-illumination. The findings in this study suggested that the electrons with high mobility produced by the front-illumination on the hydrogenated $BiVO_4$ photoanode can be efficiently transported to the conductive substrate, resulting in a significant enhancement in photocurrent generation than the pristine $BiVO_4$ photoanode. Monochromatic light PEC performance, temperature-dependent conductivity, ^{1}H NMR, and DFT calculation studies revealed that the external H atoms occupied the OVs in the $BiVO_4$ lattice facilitating the electron small polaron hopping, thus suppressing the nonradiative recombination loss of photoinduced electrons and facilitating their transport in $BiVO_4$. The observed small polaron hopping phenomenon in this work has extended the understanding of the beneficial role of hydrogen doping on metal oxides, inspiring the future development of polaronic materials in solar energy conversion.

ASSOCIATED CONTENT

Supporting Information. The Supporting Information is available free of charge at …. Detailed experimental section, supplementary XPS spectra, SEM images, XRD patterns, UV-vis plots, PL

spectra, EPR results, IPCE plots, APCE curves, gas evolution results, *J-V* curves, ^{1}H NMR spectra, and simulated results.

AUTHOR INFORMATION

Corresponding Authors

Hao Wu - Macao Institute of Materials Science and Engineering, Faculty of Innovation Engineering, Macau University of Science and Technology, Taipa, Macau, People's Republic of China; Email: wuhao@must.edu.mo; Twitter: @Andrew_Haowu

Yun Hau Ng - Low Carbon and Climate Impact Research Centre, School of Energy and Environment, City University of Hong Kong, Kowloon, Hong Kong, People's Republic of China; Email: yunhau.ng@cityu.edu.hk; Twitter: @NergyCare

Notes

The authors declare no competing financial interest.

ACKNOWLEDGMENT

H.W. and L.Z. contributed equally to this work. This project was financially supported by the Hong Kong Research Grant Council (RGC) General Research Fund (GRF) City U 11306920, CityU 11305419, and the General Program of Science and Technology Innovation Committee of Shenzhen Municipality JCYJ20190808181805621.

REFERENCES

(1) Andrei, V.; Reuillard, B.; Reisner, E. Bias-Free Solar Syngas Production by Integrating a Molecular Cobalt Catalyst with Perovskite–$BiVO_4$ Tandems. *Nat. Materials* **2019**, 19, 189-194.

(2) Kuang, Y.; Jia, Q.; Ma, G.; Hisatomi, T.; Minegishi, T.; Nishiyama, H.; Nakabayashi, M.; Shibata, N.; Yamada, T.; Kudo, A.; Domen, K. Ultrastable Low-Bias Water Splitting Photoanodes via Photocorrosion Inhibition and in Situ Catalyst Regeneration. *Nat. Energy* **2017**, *2,* 16191.

(3) Gao, R. T.; Wang, L. Stable Cocatalyst-Free $BiVO_4$ Photoanodes with Passivated Surface States for Photocorrosion Inhibition. *Angew. Chem. Int. Ed.* **2020**, *59* (51), 23094–23099.

(4) Zhou, L.; Xu, Y. F.; Chen, B. X.; Kuang, D. Bin; Su, C. Y. Synthesis and Photocatalytic Application of Stable Lead-Free $Cs_2AgBiBr_6$ Perovskite Nanocrystals. *Small* **2018**, *14* (11), 1703762.

(5) Wu, H.; Tan, H. L.; Toe, C. Y.; Scott, J.; Wang, L.; Amal, R.; Ng, Y. H. Photocatalytic and Photoelectrochemical Systems: Similarities and Differences. *Advanced Materials* **2020**, *32* (18), 1904717.

(6) Wu, H.; Irani, R.; Zhang, K.; Jing, L.; Dai, H.; Chung, H. Y.; Abdi, F. F.; Ng, Y. H. Unveiling Carrier Dynamics in Periodic Porous $BiVO_4$ Photocatalyst for Enhanced Solar Water Splitting. *ACS Energy Lett* **2021**, *6* (10), 3400–3407.

(7) Woo Kim, T.; Choi, K.-S. Nanoporous $BiVO_4$ Photoanodes with Dual-Layer Oxygen Evolution Catalysts for Solar Water Splitting. *Science (1979)* **2014**, *343* (6174), 990–994.

(8) Lee, D. K.; Choi, K. S. Enhancing Long-Term Photostability of $BiVO_4$ photoanodes for Solar Water Splitting by Tuning Electrolyte Composition. *Nat Energy* **2018**, *3* (1), 53–60.

(9) Rettie, A. J. E.; Lee, H. C.; Marshall, L. G.; Lin, J. F.; Capan, C.; Lindemuth, J.; McCloy, J. S.; Zhou, J.; Bard, A. J.; Mullins, C. B. Combined Charge Carrier Transport and Photoelectrochemical Characterization of $BiVO_4$ Single Crystals: Intrinsic Behavior of a Complex Metal Oxide. *J Am Chem Soc* **2013**, *135* (30), 11389–11396.

(10) Ziwritsch, M.; Müller, S.; Hempel, H.; Unold, T.; Abdi, F. F.; Van De Krol, R.; Friedrich, D.; Eichberger, R. Direct Time-Resolved Observation of Carrier Trapping and Polaron Conductivity in $BiVO_4$. *ACS Energy Lett* **2016**, *1* (5), 888–894.

(11) Zhang, L.; Chu, W.; Zhao, C.; Zheng, Q.; Prezhdo, O. V; Zhao, J. Dynamics of Photoexcited Small Polarons in Transition-Metal Oxides. *Journal of Physical Chemistry Letters* **2021**, *12* (9), 2191-2198.

(12) Qiu, W.; Xiao, S.; Ke, J.; Wang, Z.; Tang, S.; Zhang, K.; Qian, W.; Huang, Y.; Huang, D.; Tong, Y.; Yang, S. Freeing the Polarons to Facilitate Charge Transport in $BiVO_4$ from Oxygen Vacancies with an Oxidative 2D Precursor. *Angew. Chem. Int. Ed.* **2019**, *8*, 19087 –19095.

(13) Qu, Y.; Yang, S. Origin of the Different Photoelectrochemical Performance of Mesoporous BiVO4 Photoanodes between the $BiVO_4$ and the FTO Side Illumination. *J. Phys. Chem. C* **2015**, *119* (41), 23350–23357.

(14) Zhang, L.; Ye, X.; Boloor, M.; Poletayev, A.; Melosh, N. A.; Chueh, W. C. Significantly Enhanced Photocurrent for Water Oxidation in Monolithic Mo:$BiVO_4$/SnO_2/Si by

Thermally Increasing the Minority Carrier Diffusion Length. *Energy Environ Sci* **2016**, *9* (6), 2044–2052.

(15) Kuang, Y.; Jia, Q.; Nishiyama, H.; Yamada, T.; Kudo, A.; Domen, K. A Front-Illuminated Nanostructured Transparent $BiVO_4$ Photoanode for >2% Efficient Water Splitting. *Adv. Energy Mater.* **2016**, *6* (2), 1501645.

(16) Yang, J. W.; Park, I. J.; Lee, S. A.; Lee, M. G.; Lee, T. H.; Park, H.; Kim, C.; Park, J.; Moon, J.; Kim, J. Y.; Jang, H. W. Near-Complete Charge Separation in Tailored $BiVO_4$-Based Heterostructure Photoanodes toward Artificial Leaf. *Appl. Catal. B* **2021**, *293*, 120217.

(17) Gao, R. T.; Liu, X.; Zhang, X.; Wang, L. Steering Electron Transfer Using Interface Engineering on Front-Illuminated Robust $BiVO_4$ Photoanodes. *Nano Energy* **2021**, *89*, 106360.

(18) Wu, H.; Qu, S; Xie, Z.; Ng, Y.H. Surface Modulation Inducing Bismuth-Rich Surface Composition in $BiVO_4$ for Efficient Photoelectrochemical Water Splitting. *ACS Appl. Energy Mater.* **2022**, *5* (7), 8419-8427.

(19) Wang, S.; He, T.; Chen, P.; Du, A.; Ostrikov, K. K.; Huang, W.; Wang, L. In Situ Formation of Oxygen Vacancies Achieving Near-Complete Charge Separation in Planar $BiVO_4$ Photoanodes. *Adv. Mater.* **2020**, *32* (26), 2001385.

(20) Meng, A. Q.; Zhang, B.; Fan, L.; Liu, H.; Edström, K.; Cuartero, M.; Marco, R. De; Crespo, G. A.; Sun, L. Efficient $BiVO_4$ Photoanodes by Postsynthetic Treatment: Remarkable Improvements in Photoelectrochemical Performance from Facile Borate Modification. *Angew. Chem. Int. Ed.* **2019**, *58*, 19027 –19033.

(21) Ye, K.-H.; Li, H.; Huang, D.; Xiao, S.; Qiu, W.; Li, M.; Hu, Y.; Mai, W.; Ji, H.; Yang, S. Enhancing Photoelectrochemical Water Splitting by Combining Work Function Tuning and Heterojunction Engineering. *Nat. Commun.* **2019**, *10* (1), 3687.

(22) Chen, X.; Liu, L.; Yu, P. Y.; Mao, S. S. Increasing Solar Absorption for Photocatalysis with Black Hydrogenated Titanium Dioxide Nanocrystals. *Science (1979)* **2011**, *331* (6018), 746–750.

(23) Wang, G.; Ling, Y.; Lu, X.; Qian, F.; Tong, Y.; Zhang, J. Z.; Lordi, V.; Rocha Leao, C.; Li, Y. Computational and Photoelectrochemical Study of Hydrogenated Bismuth Vanadate. *J. Phys. Chem. C* **2013**, *117* (21), 10957–10964.

(24) Tian, Z.; Zhang, P.; Qin, P.; Sun, D.; Zhang, S.; Guo, X.; Zhao, W.; Zhao, D.; Huang, F. Novel Black $BiVO_4$ /TiO_{2-x} Photoanode with Enhanced Photon Absorption and Charge Separation for Efficient and Stable Solar Water Splitting. *Adv. Energy. Mater.* **2019**, *9* (27), 1901287.

(25) Fernández-Climent, R.; Giménez, S.; García-Tecedor, M. The Role of Oxygen Vacancies in Water Splitting Photoanodes. *Sustain. Energy Fuels* **2020**, *4*, 5916–5926.

(26) Singh, T.; Müller, R.; Singh, J.; Mathur, S. Tailoring Surface States in WO_3 Photoanodes for Efficient Photoelectrochemical Water Splitting. *Appl Surf Sci* **2015**, *347*, 448–453.

(27) Cooper, J. K.; Scott, S. B.; Ling, Y.; Yang, J.; Hao, S.; Li, Y.; Toma, F. M.; Stutzmann, M.; Lakshmi, K. V.; Sharp, I. D. Role of Hydrogen in Defining the N-Type Character of $BiVO^4$ Photoanodes. *Chem. Mater.* **2016**, *28* (16), 5761–5771.

(28) Jang, J. W.; Friedrich, D.; Müller, S.; Lamers, M.; Hempel, H.; Lardhi, S.; Cao, Z.; Harb, M.; Cavallo, L.; Heller, R.; Eichberger, R.; van de Krol, R.; Abdi, F. F. Enhancing Charge Carrier Lifetime in Metal Oxide Photoelectrodes through Mild Hydrogen Treatment. *Adv. Energy Mater.* **2017**, *7* (22), 201701536.

(29) Kim, T. W.; Ping, Y.; Galli, G. A.; Choi, K. S. Simultaneous Enhancements in Photon Absorption and Charge Transport of Bismuth Vanadate Photoanodes for Solar Water Splitting. *Nat. Commun.* **2015**, *6*, 8769.

(30) Zhang, K.; Jin, B.; Park, C.; Cho, Y.; Song, X.; Shi, X.; Zhang, S.; Kim, W.; Zeng, H.; Park, J. H. Black Phosphorene as a Hole Extraction Layer Boosting Solar Water Splitting of Oxygen Evolution Catalysts. *Nat. Commun.* **2019**, *10*, 2001.

(31) Lu, Y.; Yang, Y.; Fan, X.; Li, Y.; Zhou, D.; Cai, B.; Wang, L.; Fan, K.; Zhang, K. Boosting Charge Transport in $BiVO_4$ Photoanode for Solar Water Oxidation. *Adv. Mater.* **2022**, *34* (8), 202108178.

(32) Zhang, W.; Yan, D.; Li, J.; Wu, Q.; Cen, J.; Zhang, L.; Orlov, A.; Xin, H.; Tao, J.; Liu, M. Anomalous Conductivity Tailored by Domain-Boundary Transport in Crystalline Bismuth Vanadate Photoanodes. *Chem. Mater.* **2018**, *30* (5), 1677–1685.

(33) Zhang, Z.; Nagashima, H.; Tachikawa, T. Ultra-Narrow Depletion Layers in Hematite Mesocrystal-Based Photoanode for Boosting Multihole Water Oxidation. *Angew. Chem. Int. Ed.* **2020**, *59*, 9047 –9054.

(34) Zhang, Z.; Karimata, I.; Nagashima, H.; Sugimoto, K.; Tachikawa, T. Interfacial Oxygen Vacancies Yielding Long-Lived Holes in Hematite Mesocrystal-Based Photoanodes. *Nat. Commun.* **2019**, *10*, 4832.

(35) Garcia-Belmonte, G.; Munar, A.; Barea, E. M.; Bisquert, J.; Ugarte, I.; Pacios, R. Charge Carrier Mobility and Lifetime of Organic Bulk Heterojunctions Analyzed by Impedance Spectroscopy. *Org Electron* **2008**, *9* (5), 847–851.

(36) Zhang, C.; Xie, Y.; Bai, T.; Hu, J.; Wang, J. Cooperation of Multifunction Composite Structures and Fluorescein for Photovoltaic Performance-Enhanced ZnO-Based Dye-Sensitized Solar Cells. *J. Power Sources* **2015**, *297*, 16–22.

(37) Vernon, S. M.; Anderson, W. A. Temperature Effects in Schottky-Barrier Silicon Solar Cells. *Appl. Phys. Lett.* **1975**, *26* (12), 707–709.

(38) Li, D.; Liu, Y.; Shi, W.; Shao, C.; Wang, S.; Ding, C.; Liu, T.; Fan, F.; Shi, J.; Li, C. Crystallographic-Orientation-Dependent Charge Separation of $BiVO_4$ for Solar Water Oxidation. *ACS Energy Lett* **2019**, *4* (4), 825–831.

(39) Eichhorn, J.; Reyes-lillo, S. E.; Roychoudhury, S.; Sallis, S.; Weis, J.; Larson, D. M.; Cooper, J. K.; Sharp, I. D.; Prendergast, D.; Toma, F. M. Revealing Nanoscale Chemical Heterogeneities in Polycrystalline Mo-$BiVO_4$ Thin Films. *Small* **2020**, *16* (35), 2001600.

(40) Wiktor, J.; Ambrosio, F.; Pasquarello, A. Role of Polarons in Water Splitting: The Case of $BiVO_4$. *ACS Energy Lett* **2018**, *3* (7), 1693–1697.

(41) Zhang, W.; Wu, F.; Li, J.; Yan, D.; Tao, J.; Ping, Y.; Liu, M. Unconventional Relation between Charge Transport and Photocurrent via Boosting Small Polaron Hopping for Photoelectrochemical Water Splitting. *ACS Energy Lett.* **2018**, *3* (9), 2232–2239.

(42) Patil, D. S.; Konale, M.; Cozic, S.; Calvez, L.; Zima, V.; Wagner, T.; McCloy, J. S.; le Coq, D. Percolation Behavior of Ag in Ge16Sb12Se72 Glassy Matrix and Its Impact on Corresponding Ionic Conductivity. *J. Alloys. Compd.* **2019**, *782*, 375–383.

(43) Pradhan, D. K.; Kumari, S.; Puli, V. S.; Das, P. T.; Pradhan, D. K.; Kumar, A.; Scott, J. F.; Katiyar, R. S. Correlation of Dielectric, Electrical and Magnetic Properties near the Magnetic Phase Transition Temperature of Cobalt Zinc Ferrite. *Phys. Chem. Chem. Phys.* **2017**, *19* (1), 210–218.

(44) Khadhraoui, S.; Triki, A.; Hcini, S.; Zemni, S.; Oumezzine, M. Variable-Range-Hopping Conduction and Dielectric Relaxation in $Pr_{0.6}Sr_{0.4}Mn_{0.6}Ti_{0.4}O_{3\pm\delta}$ Perovskite. *J. Magn. Magn. Mater.* **2014**, *371*, 69–76.

(45) Deshpande, S. K.; Shrikhande, V. K.; Jugad, M. S.; Goyal, P. S.; Kothiyal, G. P. Conductivity Studies of Lithium Zinc Silicate Glasses with Varying Lithium Contents. *Bull. of Mater. Sci.* **2007**, *30* (5), 497–502.

(46) Wu, H.; Zhang, L.; Du, A.; Irani, R.; van de Krol, R.; Abdi, F. F.; Ng, Y. H. Low-Bias Photoelectrochemical Water Splitting via Mediating Trap States and Small Polaron Hopping. *Nat. Commun.* **2022**, *13*, 6231.

(47) Walsh, A.; Yan, Y.; Huda, M. N.; Al-Jassim, M. M.; Wei, S.-H. Band Edge Electronic Structure of $BiVO_4$: Elucidating the Role of the Bi *s* and V *d* Orbitals. *Chem. Mater.* **2009**, *21* (19), 547–551.

(48) Tang, S.; Qiu, W.; Xu, X.; Xiao, S.; Tong, Y.; Wang, X.; Yang, S. Harvesting of Infrared Part of Sunlight to Enhance Polaron Transport and Solar Water Splitting. *Adv. Funct. Mater.* **2022**, *32* (18), 2110284.

(49) Zachäus, C.; Abdi, F. F.; Peter, L. M.; Van De Krol, R. Photocurrent of $BiVO_4$ Is Limited by Surface Recombination, Not Surface Catalysis. *Chem. Sci.* **2017**, *8* (5), 3712–3719.